TÜBİTAK

Turkish Journal of Physics

http://journals.tubitak.gov.tr/physics/

Research Article

Turk J Phys
(2018) 42: 33 – 40

doi:10.3906/fiz-1706-22

Surface effect in explaining the elastic scattering of the α+^{12}C system at low energies

Yasemin KÜÇÜK*
Department of Physics, Akdeniz University, Antalya, Turkey

Received: 19.06.2017 • **Accepted/Published Online:** 09.10.2017 • **Final Version:** 13.02.2018

Abstract: In this paper, the elastic scattering angular distributions data of the α+12C reaction at an energy range of 13.0 to 172.5 MeV were analyzed within the framework of optical model formalism. A phenomenological deep real potential was used with a phenomenological Woods–Saxon type imaginary potential. Excellent agreement was obtained in the high-energy region. The phenomenological deep potential was unable to explain the experimental data in the low-energy region. The experimental data at both low and high energies could not be explained at the same time. In order to explain the data simultaneously at low energy and high energy, the shape of the deep real potential was modified in the surface region. This work shows the role of the surface region of two nuclei in explaining the elastic scattering data of this system.

Key words: Optical model, deep potential, elastic scattering

1. Introduction

The formation of elements starts charged-particle reactions, induced by α-particles. Therefore, the interactions of this particle with light-heavy ions bear significance in nuclear physics and nuclear astrophysics. One of the most important interactions is the α+^{12}C reaction. It has attracted considerable interest and has been studied both experimentally and theoretically over the years. A large body of data has been accumulated as a result of this intense research. In general, the theoretical studies have divided the experimental data into two energy regions, high and low ones, and they have been studied separately by using various models.

The elastic scattering of α particles from ^{12}C nuclei has been analyzed for the low-energy region by some authors [1–7]. Carter et al. [1] examined the low-energy data using the standard optical model and a modified smooth cut-off model, called the APBM model, and showed that the shallow Woods–Saxon potential is not adequate to explain the experimental data. They were able to explain the experimental data for the laboratory energies between 10.0 and 19.0 MeV by using the APBM cut-off model. However, they have not applied this model to higher energies. For high-energy data, models based on the folded potentials have been used in general [8–10]. In these studies, a satisfactory agreement with experimental data was obtained by using the double-folding models at some incident energies in the high energy region. Yang et al. [11] conducted a detailed analysis of the elastic scattering data over a wide energy range, from 13.0 to 172.5 MeV, using a folding model based on an α-particle model. They obtained good agreement for angular distributions at the high-energy region between 90.0 and 172.5 MeV. Although their model is adequate to fit the data for intermediate energies, fit to the details of the experimental data could not be achieved. They examined the low-energy data

*Correspondence: ykucuk@akdeniz.edu.tr

and showed that their model had the worst results at the low-energy region in comparison with the intermediate and high-energy region data (see Ref. [11] for details).

It may be perceived from all these studies that the α+^{12}C system is very difficult and there are some problems to be addressed in explaining the elastic scattering data, especially in the low-energy region. The models used until now have not provided a consistent description for all data measured so far. In the light of these, this study aimed to explain the experimental data of the α+^{12}C reaction by using a deep Woods–Saxon squared real potential with a shallow Woods–Saxon imaginary potential over a wide energy range from 13.0 to 172.5 MeV within the framework of the optical model formalism.

In the following section, the optical model is given with the potential parameters used to analyze the experimental data of the α+^{12}C system. In Section 3, the results of these analyses are presented. A summary and conclusion are given in the last section.

2. Model

The form of the potential, which represents the two-body interaction between the projectile and the target nucleus, is of great significance in the optical model calculations. The potential can be obtained microscopically by using the density distributions of the interacting nuclei with an effective interaction via the folding model similar to [12], or a phenomenological form may be chosen [13]. In this work, the phenomenological Woods–Saxon form was chosen for the optical potential in this analysis. The WS form is flexible, since it has three adjustable parameters (depth, radius, and diffuseness), whereas the folding potential has only one adjustable parameter, the normalization factor, N_R.

The optical potential can be expressed as follows:

$$V_{total}(r) = V_{Nuclear}(r) + V_{Coulomb}(r) + V_{Centrifugal}(r) \tag{1}$$

The Coulomb potential is due to a charge $Z_P e$ interacting with a charge $Z_T e$ distributed uniformly over a sphere of radius R_c

$$V_{Comb}(r) = \frac{1}{4\pi\varepsilon_0}\frac{Z_P Z_{Te^2}}{r} \quad r > R_C \tag{2}$$

$$V_{Comb}(r) = \frac{1}{4\pi\varepsilon_0}\frac{Z_P Z_{Te^2}}{2R_c}\,(3 - \frac{r}{R_c^2}) \quad r < R_C, \tag{3}$$

where R_C is the Coulomb radius, and Z_P and Z_T denote the charges of the projectile and the target nuclei, respectively.

The nuclear potential consists of real and imaginary potentials, given as

$$V_{Nuclear}(r) = \frac{-V_0}{1+e^{\frac{r-R_v}{a_v}}} + \frac{-W_0}{1+e^{\frac{r-R_w}{a_w}}} \tag{4}$$

$R_v = r_v[A_p + A_T]$ and $R_w = r_w[A_p + A_T]$. Here A_p is the mass of projectile and A_T is the mass of the target. The variable r shows the radius parameters of the real and imaginary parts of the potential. The real potential is the square of the Woods–Saxon shape with the depth $V_0 = 295.0$ MeV, which is constant for all calculations. The diffuseness parameter has been fixed to two different values. For high-energy regions between 90.0 and 172.5 MeV, $a_V = 1.65$ fm and for low-energy regions between 13.0 and 60.0 MeV, $a_V = 1.45$ fm. The

Table 1. The parameters and volume integrals of the real and imaginary potentials of the optical model calculations.

E_{LAB} (MeV)	r_V (fm)	W (fm)	J_V (MeVfm^3)	$J_{W\,b}$(MeVfm^3)
13.0	0.30	1.5	127.6	20.8
18.0	0.76	2.0	606.3	27.3
22.0	0.71	7.3	521.6	101.2
29.0	0.71	5.0	521.6	69.4
41.0	0.70	9.0	505.9	124.9
48.7	0.70	11.0	505.9	152.6
54.1	0.70	11.0	505.9	152.6
60.0	0.71	12.0	521.6	166.5
90.0	0.39	6.0	221.2	83.2
104.0	0.45	7.0	268.2	97.1
120.0	0.39	6.0	221.2	83.2
139.0	0.39	7.0	221.2	97.1
145.0	0.37	6.0	221.2	83.2
166.0	0.33	6.0	180.9	83.2
172.5	0.30	5.0	163.4	69.4

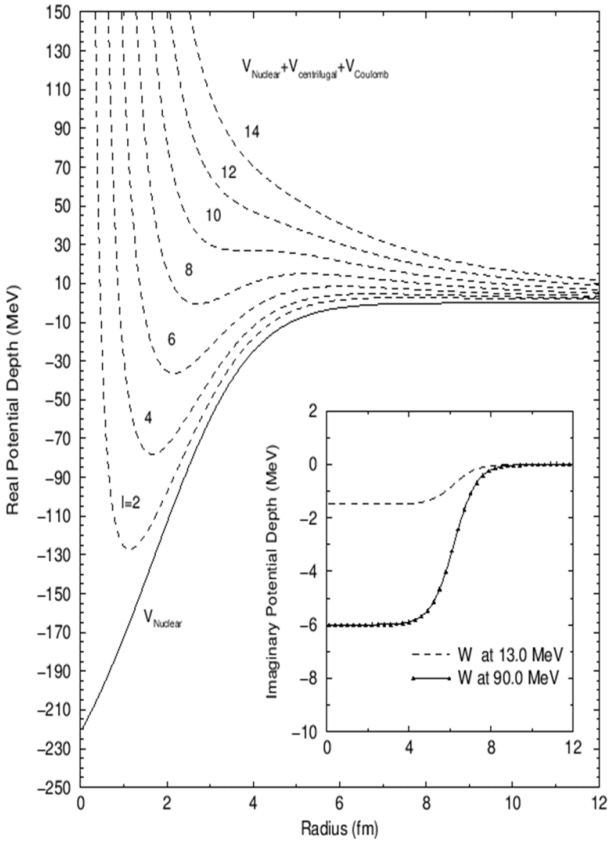

Figure 1. The interaction potential between ^{4}He and ^{12}C is plotted against the separation R for various values of the orbital angular momentum quantum number, l. The inserted figure shows the imaginary potential at E_{Lab} = 13.0 and 90.0 MeV. The parameters are given in the text.

radius parameters vary with energy, as given in Table 1. The real part of the nuclear potential and the total potential are displayed in Figure 1 for various values of the orbital angular momentum.

The imaginary potential has the Woods–Saxon volume shape. The depths, W_0, are given in Table 1. The radius and diffusions parameters of the imaginary potential have also been fixed in the calculations as $r_W = 1.35$ fm and $a_W = 0.55$ fm. Figure 1 shows the imaginary part of the nuclear potential. The volume integrals of the real and imaginary potentials are shown in Table 1. For all calculations, the code Fresco was used [14].

3. Results and discussion

Fifteen elastic angular distributions of the $\alpha+^{12}$C system from 13.0 to 172.5 MeV were analyzed. At first, the double folding model was used to examine the data and results similar to those reported by Yang et al. [11] were obtained: good agreement with the experimental data at high energies, but poor agreement with the low-energy data. The agreement could not be improved by varying N_R. Then the Woods–Saxon squared form described in the previous section was used for the real part of the nuclear potential, which shows a similar behavior with the folded potential.

The phenomenological Woods–Saxon potential family gave very good agreement at high energies, as shown in Figure 2. However, this potential family failed to provide an agreement with the data at low energies. The results are very similar to the findings reported by Yang et al. [11] obtained by using the double folding potential. These results are shown in Figures 3 and 4 with dashed lines. Neither microscopic nor phenomenological deep potentials provide a consistent description of the experimental data.

Because of the failure of the microscopic and phenomenological potentials, the sensitivity of the real potential was examined to explain the scattering observables of this reaction. For this purpose, a notch test was performed. A Woods–Saxon derivative potential with a small depth was used at different radius points. The potential has no effect on the scattering for a radius of 4 fm. However, after 4 fm, it affects the phases of the oscillation in the cross-section. Therefore, by conducting a detailed study, the shape of the real potential in the surface region of the nuclear potential was modified by adding two small potentials at different radial points [15]. These points, where two small potentials are included, are close to the touching distance of the two nuclei. This shows that these types of reactions involve surface effects. These two small additional potentials are derivatives of the Woods–Saxon shape.

Therefore, the total real potential for these calculations consists of the nuclear potential, $V_{Nuclear}$, with two small additional potentials:

$$V_{total}(r) = V_{Nuclear}(r) + U(r) + V_{Coulomb}(r) + V_{Centrifugal}(r) \tag{5}$$

$$U(r) = 4U_1 a_1 \frac{df(r, R_1, a_1)}{dr} + 4U_2 a_2 \frac{df(r, R_2, a_2)}{dr} \tag{6}$$

$$F(r, R, a) = \frac{1}{[1 + e^{\frac{r-R}{a}}]} \tag{7}$$

Two small potentials are shown in Figure 5 and the parameters are shown in Table 2. By adding these small potentials to the phenomenological Woods–Saxon squared nuclear potential, better agreement with the experimental data was obtained. As clearly seen in Figures 3 and 4, satisfactory agreement was obtained between the theoretical results and the experimental data in the low-energy region. These results are better than the microscopic and phenomenological potential results obtained so far in the literature. When these results are

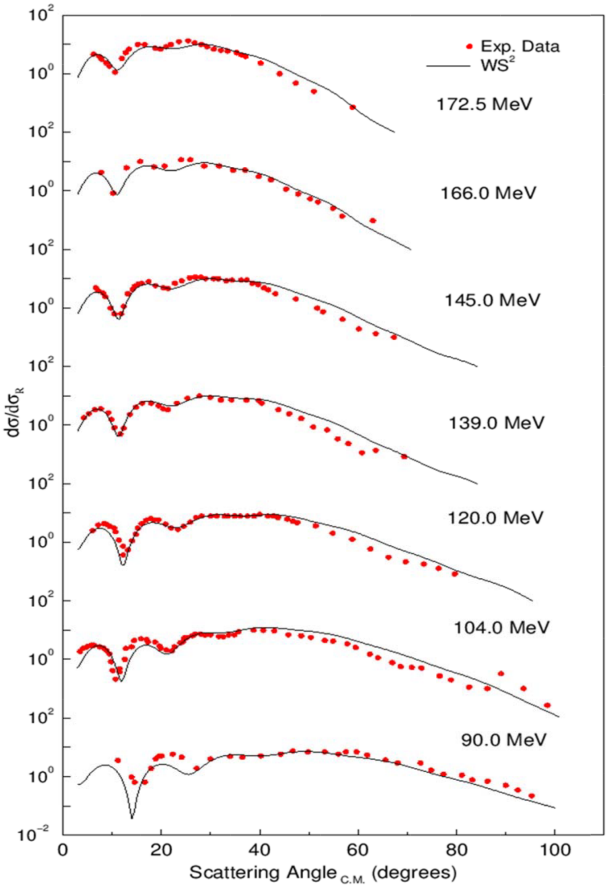

Figure 2. The elastic scattering angular distributions obtained by using the optical model for the α+^{12}C system. The experimental data are taken from [1,2,4].

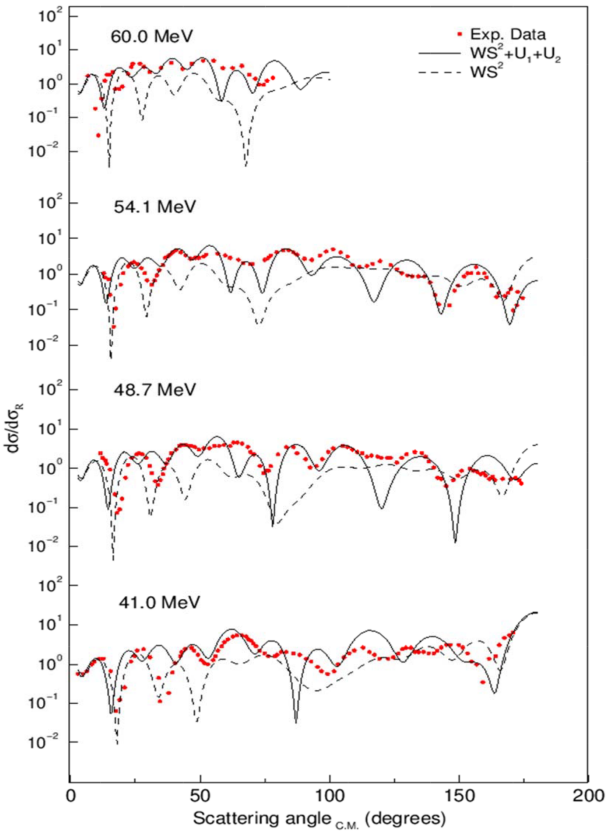

Figure 3. The elastic scattering angular distributions obtained by using the optical model for the α+^{12}C system. Here the solid lines show the modified optical potential and dashed lines show the standard optical potential. The experimental data shown in circles are taken from [3,5,6].

compared with the results obtained by Yang et al. [11], who analyzed these data with a folded potential, the fits in this paper are more favorable. It should be emphasized here that in the present calculations only two parameters, the radius of the real potential and the depth of the imaginary potential, have been changed with the energy to improve the quality of the fits. The parameters are displayed in Table 1 and the other parameters, which are given in Section 2, are kept constant in all calculations.

Table 2. The parameters of the two small additional potentials.

U_1 (MeV)	R_1 (fm)	a_1 (fm)	U_2 (MeV)	R_2 (fm)	a_2 (fm)
11.0	1.1	0.1	4.5	1.52	0.511

The results show that two small potentials have a significant effect in explaining the low-energy data. Although their depths are not deep, they have a large effect on the scattering. This is also clearly seen in Figure 6, where we show the far- and near-side components of the total cross-section. These additional potentials contribute to the interference between the inner wave comes from the reflection at the inner face of the total

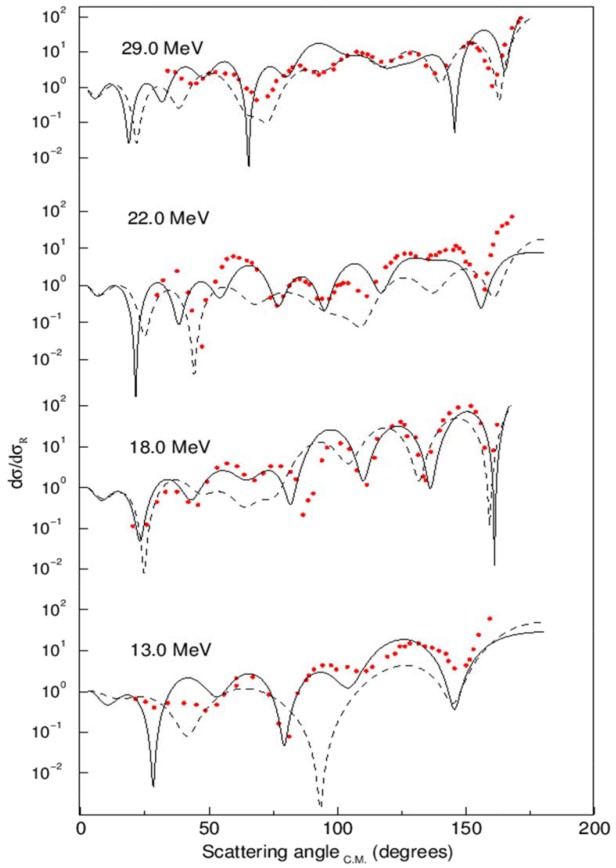

Figure 4. The elastic scattering angular distributions obtained by using the optical model. Here the solid lines show the modified optical potential and the dashed lines show the standard optical potential. The experimental data shown in circles are taken from [7].

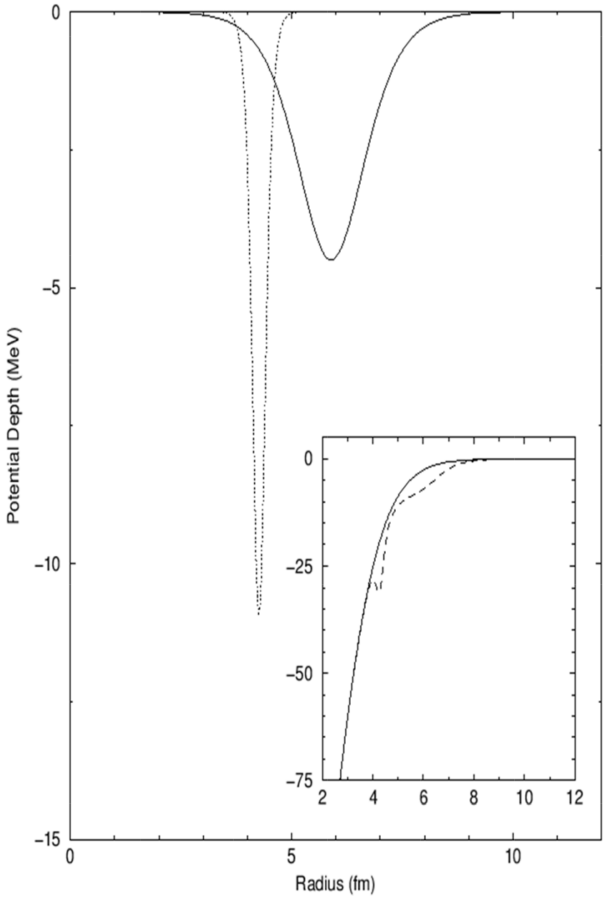

Figure 5. The shapes of two small potentials $U_1(r)$ and $U_2(r)$ are displayed by dotted and solid lines, respectively. The inset shows their effects on the nuclear potential with a long-dashed line.

potential pocket and external wave comes from the reflection at the outer barrier [15–17] (see Figure 1 for the pocket in the total real potential). These small potentials affect also the magnitudes and phases of the internal and external waves. However, when the potential pocket disappears for the high angular momentum number l, which may be called the "grazing angular momentum" or l_g, the interference between the internal and external waves loses the importance [18,19]. Therefore, $l_g > 10$, which corresponds to an E_{lab} of approximately 60 MeV, and the total potential pocket seen in Figure 1 disappears. As a result, these small potentials have no effect on l_g, this energy, and can be ignored at the higher-energy region. Therefore, these small potentials above 60 MeV were removed and the Woods–Saxon squared potential was used by adjusting the diffuseness to $a_V = 0.65$ fm, without changing other parameters, in order to provide quality of fit. These results can also be discussed in the light of findings reported by Baye [20]. He investigated nucleus–nucleus scattering within the framework of supersymmetric quantum theory and showed the relation between deep and shallow potentials. He also showed that both shallow and deep potentials are phase equivalent, and thus different deep and shallow interaction potentials give similar elastic cross-sections. The surface effects of the Woods–Saxon potentials for the scattering have also been discussed in [21–23].

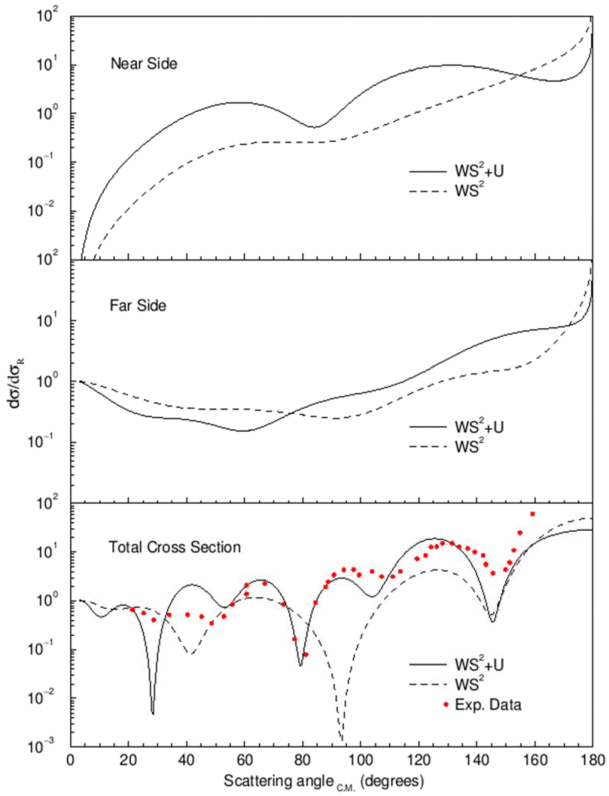

Figure 6. The near- and far-side components of the total cross-section. The interference of the near- and far-side components gives the total cross-section in the figure.

4. Summary and conclusion

In this paper, the elastic scattering of the α+^{12}C system was analyzed over a wide energy range from 13.0 to 172.5 MeV in a laboratory system using an optical model. This study aimed to explain the experimental data in the low- and high-energy regions simultaneously and to improve the theoretical results obtained by using the microscopic and phenomenological potentials [8]. In the high-energy region, a good agreement with the experimental data similar to previous works in the literature was obtained using the deep Woods–Saxon squared potential. However, this potential could not provide a satisfactory description of the experimental data in the low-energy region. These results are again similar to the previous works conducted so far in the literature. Nevertheless, an improved agreement with the experimental data was obtained by modifying the shape of the phenomenological Woods–Saxon squared potential in the surface region.

These analyses demonstrate two important results. First, the real potential must be deep to create a pocket in the total potential, as shown in Figure 1. Secondly, the imaginary potential should be weak enough to let the interference between the inner waves coming from the inner barrier and external waves coming from Coulomb barrier for the angular momentum numbers be less than the grazing one. This paper has also shown that the shape of the nuclear potential in the surface region has crucial importance in explaining the scattering observables for the α+^{12}C system. Consequently, two small potentials added to the surface region clearly take into account the surface effects of two touching nuclei and satisfactory agreement has been obtained at low energies by using this model. The same effect also observed in the system of ^{16}O +^{28}Si [16]. It shows that elastic scattering is very sensitive to the surface regions at low energies for the light systems, as investigated in this paper.

References

[1] Carter, E. B.; Mitchel, G. E.; Davis. R. H. *Phys. Rev.* **1964**, *133*, 1421-1433.

[2] Oeschler, H.; Fuchst, H.; Schröter, H. *Nucl. Phys. A* **1973**, *202*, 513-529.

[3] Abele, H. E.; Hauser, H.; Körber, A.; Leitner, W.; Neu, R., Plappert, H.; Rohwer, T.; Staudt, G.; Strasser, M.; Welte, S.; et al. *Z. Phys. A*. **1987**, *326*, 373-381.

[4] Baron, N.; Leonard, R. F.; Steward, W. M. *Phys. Rev. C* **1971**, *4*, 1159-1173.

[5] Buenerd, M., Martin, P.; De Saintignon, P.; Loiseaux, J. M. *Nucl. Phys. A* **1977**, *286*, 377-402.

[6] Yasue, M.; Tanabe, T.; Kokame, J.; Soga, F.; Shimokoshi, F.; Kasagi, J.; Toba, Y.; Kadota, Y.; Ohsawa, T.; Furuno, K. *Nucl. Phys. A* **1983**, *394*, 29-38.

[7] Lichtenthaler, R.; Villari, A. C. C.; Lepine-Szily, A.; Gomes, L. C. *Phys. Rev. C* **1991**, *44*, 1152-1155.

[8] Khoa, D. T., *Nucl. Phys. A* **1988**, *484*, 376-396.

[9] Khallaf, S. A.; Amry, A.; Mokhtar, S. R. *Phys. Rev. C* **1997**, *56*, 2093-2103.

[10] Khoa, D. T. *Phys. Rev. C* **2001**, *63*, 034007, 1-15.

[11] Yang, Y.; Li, Q. *Nuc. Phys. A* **2004**, *732*, 3-12.

[12] Karakoc, M.; Boztosun, I. *Phys. Rev. C* **2006**, *73*, 047601, 1-4.

[13] Boztosun, I; Bayrak, O.; Dagdemir, Y. *Int. Jour. Mod. Phys. E* **2005**, *14*, 663-673.

[14] Thompson, I. *Comput. Phys. Rep.* **1988**, *7*, 167-212.

[15] Boztosun, I. *Phys. Rev. C* **2002**, *66*, 024610, 1-11.

[16] Kobos, A. M.; Satchler, G. R.; Mackintosh, R. S. *Nucl. Phys. A* **1983**, *395*, 248-262.

[17] Lee, S. Y. *Nucl. Phys. A* **1978**, *311*, 518-532.

[18] Brink, D. M.; Takigawa, N. *Nucl. Phys. A* **1977**, *279*, 159-188.

[19] Boztosun, I.; Rae, W. D. M. *Phys. Lett. B* **2001**, *518*, 229-234.

[20] Baye, D. *Phys. Rev. Lett.* **1987**, *58*, 2738-2741.

[21] Çapak, M.; Petrellis, D.; Gönül, B.; Bonatsos, D. *J. Phys. G: Nucl. Part. Phys.* **2015**, *42*, 095102, 1-24.

[22] Çapak, M.; Petrellis, D.; Gönül, B. *Mod. Phys. Lett. A* **2016**, *31*, 1650134, 1-7.

[23] Gönül, B.; Köksal, K. *Phys. Scr.* **2007**, *76*, 565-570.